Journal of Colloid and Interface Science 607 (2022) 1466–1477

Contents lists available at ScienceDirect

Journal of Colloid and Interface Science

journal homepage: www.elsevier.com/locate/jcis

Hybrid thermoresponsive nanoparticles containing drug nanocrystals for NIR-triggered remote release

Teresa Alejo [a,b,*], Victor Sebastian [a,b,c,d], Gracia Mendoza [c,d], Manuel Arruebo [a,b,c,d]

[a] Instituto de Nanociencia y Materiales de Aragón (INMA), CSIC-Universidad de Zaragoza, Zaragoza 50009, Spain
[b] Department of Chemical Engineering, University of Zaragoza, Campus Río Ebro - Edificio I+D, C/ Poeta Mariano Esquillor S/N, 50018 Zaragoza, Spain
[c] Networking Research Center on Bioengineering, Biomaterials and Nanomedicine, CIBER-BBN, 28029 Madrid, Spain
[d] Aragon Health Research Institute (IIS Aragón), 50009 Zaragoza, Spain

GRAPHICAL ABSTRACT

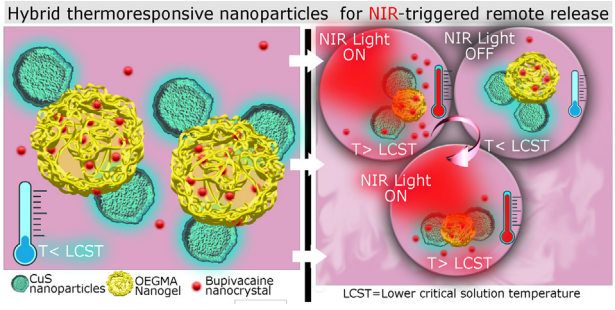

ARTICLE INFO

Article history:
Received 27 May 2021
Revised 23 August 2021
Accepted 12 September 2021
Available online 17 September 2021

Keywords:
NIR-activated nanoparticles
Reversible thermoresponsive nanogels
On–off switching release
Bupivacaine nanocrystals
Drug delivery

ABSTRACT

The on-demand administration of anaesthetic drugs can be a promising alternative for chronic pain management. To further improve the efficacy of drug delivery vectors, high drug loadings combined with a spatiotemporal control on the release can not only relief the pain according to patient's needs, but also improve the drawbacks of conventional burst release delivery systems. In this study, a hybrid nanomaterial was developed by loading bupivacaine nanocrystals (BNCs) into oligo(ethylene glycol) methyl ether methacrylate (OEGMA)-based thermoresponsive nanogels and coupling them to NIR-absorbing biodegradable copper sulphide nanoparticles (CuS NPs). Those CuS NPs were surface modified with polyelectrolytes using layer-by-layer techniques to be efficiently attached to the surface of nanogels by means of supramolecular interactions. The encapsulation of bupivacaine in the form of nanocrystals allowed to achieve CuS@BNC-nanogels having drug loadings as high as 65.5 wt%. The nanocrystals acted as long-lasting drug reservoirs, leading to an elevated localized drug content, which was useful for their application in prolonged pain relief. The CuS@BNC-nanogels exhibited favorable photothermal transducing properties upon NIR-light irradiation. The photothermal effect granted by the CuS NPs triggered the nano-crystallized drug release to be boosted by the collapse of the thermoresponsive nanogels upon heating. Remote control was achieved for on-demand release at a specific time and place, indicating their potential use as an externally activated triggerable drug-delivery system. Furthermore, cell viability tests and flow cytometry analysis were performed showing satisfactory cytocompatibility in the dose-ranging study having a subcytotoxic concentration of 0.05 mg/mL for CuS@BNC-nanogels. This remotely activated nanoplatform is a promising strategy for long-lasting controlled analgesia and a potential alternative for clinical pain management.

* Corresponding author.
E-mail address: teresaal@unizar.es (T. Alejo).

https://doi.org/10.1016/j.jcis.2021.09.064
0021-9797/

1. Introduction

The treatment of chronic pain remains challenging. Conventional treatments for pain management are based on opioids and non-steroidal anti-inflammatory drugs (NSAIDs), that usually have associated numerous side effects [1]. Local anesthetics (LA) such as lidocaine, bupivacaine and ropivacaine that block the conduction of nerve impulses in the peripheral nervous system are extensively used for surgical pain control and postoperative pain management [2]. However, the limitations associated with LA are the commonly reported cardiovascular and neurological associated toxicities and the short duration of anesthesia, with half-times of 12–24 h, which requires a continuous injected administration of the drug [3]. Encapsulation of LA in nanoparticle-based drug delivery systems have been proposed to shorten the onset, prolong their acting time and reduce their toxicity [4]. Therefore, the development of alternative platforms that administrate the anesthetic in an on-demand manner could increase the anesthesia duration and reduce the adverse side effects together with an increased patients' adherence to the treatment facilitating a superior efficiency of the therapeutic approach. In particular, the use of responsive drug delivery systems is proposed as a potential strategy for controlled drug administration and prolonged anesthetic effect [5,6]. The chosen anesthetic dose at a convenient time and delivered to the selected site can be achieved using externally activated stimulus-responsive nanoparticles [7]. This approach would reduce the dose of anesthetic required to relief the pain and allow to modulate the degree of anesthesia according to patient's changing needs, improving the therapeutic effect [8]. Different external stimuli have been used to activate drug release such as magnetic fields, ultrasound or light [9,10]. Near-infrared (NIR) light is a promising method for remote triggering because of the possibility to modulate the fluence and time of irradiation controlling the release of the drug. Moreover, NIR-light has the best penetration depth through soft-tissues and produces less thermal damage, as it is much less absorbed by water and tissue chromophores than UV and visible lights [11,12]. NIR light can be used for the photothermal activation of thermoresponsive materials coupled to light-absorbing nanoparticles. Copper sulphide nanoparticles (CuS NPs) have received much attention due to their favorable biocompatibility, biodegradability, easy preparation and low cost [13]. After exposure to NIR-light, CuS NPs can rapidly convert light energy into heat for photothermal therapy (PTT) and as diagnostic agent in photoacoustic imaging [14]. CuS NPs can act as transducers to efficiency transform optical energy into thermal energy and when attached to a thermoresponsive polymeric material that undergoes a temperature transition, it is possible to release the transported payload [15]. Oligo(ethylene glycol) methyl ether methacrylate (OEGMA)-based copolymers are widely used for biomedical applications due to their low cytotoxicity and reversible and tunable lower critical solution temperature (LCST) [16]. One of their advantages is that the LCST can be easily adjusted by varying the ratio of monomers used [17].

Up to now, several classes of hybrid organic–inorganic nanomaterials have been explored as NIR-triggered drug delivery systems. Wang *et al.*[18] developed a platform containing plasmonic gold nanoparticles (AuNPs) and gold nanorods (AuNRs) embedded in polyacrylamide hydrogel which are cross-linked by bis-acrylamide and nucleic acid duplexes. Upon light activation, the Au nanostructures produced the heating of the hydrogels and the reversible dehybridization of the DNA duplexes, generating a more porous structure in the material, opening the DNA-based cross-linker and allowing the release of the drug. In addition, plasmonic nanoparticles such as hollow gold nanoparticles (HGNPs) [19], AuNRs [20] or gold nanocages [21] have been used as transducers to remotely trigger the disruption of a thermosensitive liposome or the phase transition of a polymer, expelling the drug contained within. For instance, gold nanocages coated with the thermoresponsive polymer poly(*N*-isopropylacrylamide) (pNIPAm) were loaded with doxorubicin (DOX) being the drug released when irradiated NIR-light collapsed the polymeric shell [22]. PNIPAm microparticles containing HGNPs and bupivacaine were developed using a novel one-step microfluidic synthesis and validated for NIR-light activated bupivacaine release [23]. A different configuration of the hybrid nanomaterial has been designed containing hybrid PNIPAm-based nanogels decorated with HGNPs on their surface to trigger the release of the anesthetic bupivacaine [24]. The photothermal heating induced by HGNPs functionalized with a shell of OEGMA-based nanogel was able to produce the collapse of the polymeric shell thus causing the release of the local anesthetic bupivacaine in a spatiotemporally controlled way [25]. CuS NPs have also been functionalized with an amino-terminated OEGMA polymers to obtain a breakable nanocomposite able to release a carried drug on-demand after NIR-light triggering [15]. Despite all this progress achieved in recent years, nanocarriers have shown moderately low drug-loading contents that usually are less than 10 wt% [15,25–27]. Future effort to create efficient nanoparticle-based drug delivery systems having clinical translation will likely hinge on designing high-drug content NPs with an enhanced drug to nanomaterial ratio. Drug nanocrystallization could offer the possibility to overcome the limited drug-loading capacity of many nanomedicines, which is a mayor challenge in the development of pharmaceutical products [28]. In our previous work, bupivacaine nanocrystals were successfully obtained and encapsulated for the first time in thermoresponsive nanogels. These novel nanosystems were able to achieve excellent drug contents and prolonged peripheral nerve block in preclinical models [29].

In this study, CuS NPs were coupled by electrostatic interactions to thermoresponsive nanogels loaded with bupivacaine nanocrystals to enhance the drug-loading content of the carrier. The photothermal ability of CuS NPs@nanogels was used to trigger the release of the nano-crystallized contained drug with the aid of remotely applied NIR light. To the best of our knowledge, this is the first investigation reporting the externally triggered release of encapsulated drug nanocrystals. Cell viability tests and flow cytometry studies were carried out in four different cell lines to evaluate the potential applications of the vector in the biomedical field.

2. Materials and methods

2.1. Materials

Di(ethylene glycol) methyl ether methacrylate (MEO_2MA, 95%), poly(ethylene glycol) methyl ether methacrylate ($OEGMA_{500}$, *Mn* 500), ethylene glycol dimethacrylate (EGDMA, >98%), sodium dodecyl sulfate (SDS, ≥98%), potassium persulfate (KPS, ≥99%), copper(II) chloride dihydrate (ACS reagent, ≥ 99.0%), sodium sulfide nonahydrate (≥99.99%), poly(vinylpyrrolidone) K30 (PVP K30, 40,000 Da), hydrazine 35 wt% in water, sodium hydroxide (NaOH, reagent grade, ≥98.0%), poly(allylamine hydrochloride) (PAH, Mw ∼ 17,500 Da), sodium (polystyrene sulfonate) (PSS, Mw ∼ 70,000 Da), sodium chloride (NaCl, ACS reagent), hydroxypropyl methylcellulose (HPMC, Mn ∼ 10,000 Da), poly(ethylene glycol) (PEG300, Mn 300 Da), bupivacaine hydrochloride monohydrate (≥99%) and (S)-(-)-limonene (96%) were purchased from Sigma-Aldrich. All of these chemicals were used as received.

2.2. Preparation of bupivacaine free base

Bupivacaine free base was synthesized using the procedure previously described in the literature [30] with slight modifications. Briefly, 50 mL of an aqueous solution of bupivacaine hydrochloride at 20 mg/mL was treated with 0.2 M NaOH solution added dropwise under stirring to obtain the bupivacaine free base. The NaOH solution was continuously added until a pH of 11 was obtained (pK_a 8.4), resulting in the precipitation of the free base form as an off-white solid. Bupivacaine free base was purified filtering the solid under vacuum and subsequently with several washes with MilliQ water to eliminate salt residues. The solid was dried under vacuum overnight, resulting in a 70 wt% synthesis yield. Its melting point was determined by differential scanning calorimetry (DSC), corroborating the production of the free base (m.p. = 107–108 °C).

2.3. Synthesis of bupivacaine nanocrystals (BNCs)

Bupivacaine nanocrystals were prepared using the anti-solvent precipitation technique reported in our previous work [29]. Hence, 50 mg of bupivacaine free base were dissolved in 1.5 mL of PEG 300. The anti-solvent solution was prepared dissolving 100 mg of the HPMC polymer in 3.5 mL of water. The HPMC aqueous solution was obtained heating it at 80 °C under stirring and subsequent cooling it down in an ice bath until the HPMC became water soluble. Bupivacaine free base dissolved in PEG300 was quickly added to the HPMC solution under continuous stirring at 400 rpm and room temperature during 2 min. The final ratio of organic and aqueous phases was maintained at 3/7, where HPMC was 2% w/w in the final dispersion. When the drug solution was added, the clear solution turned into a stable opaque dispersion showing the formation of BNCs. The final dispersion was centrifuged at 25000 rpm during 40 min using an ultracentrifuge (Beckman Coulter, Avanti J-20 XP equipped with JA25.50 rotor, USA), the supernatant was replaced with water and the solid redispersed. The BNCs were further washed by centrifugation to remove the excess of unreacted polymer. Finally, the obtained BNCs were dispersed in 5 mL of deionized water.

2.4. Loading of BNCs on thermoresponsive nanogels

Thermoresponsive P(MEO_2MA-*co*-$OEGMA_{500}$) nanogels loaded with BNCs were prepared using the aqueous precipitation polymerization method by *in situ* free radical copolymerization based on the protocol described in our previous work [29]. The drug-loaded nanogels were grown introducing the as-prepared BNCs in the nanogel synthesis beaker. Briefly, the synthesis was accomplished in a 100 mL Schlenk tube where the as-prepared BNCs were mixed with 1.56 mmol of MEO_2MA monomer, 0.21 mmol of $OEGMA_{500}$ monomer and 0.06 mmol of EGDMA as crosslinker. To maintain the lower critical solution temperature (LCST) of the nanogels in the physiological range we used a [MEO_2MA]/[$OEGMA_{500}$] monomer molar ratio of 88/12 [16]. The volume phase transition temperature (VPTT) of the obtained nanogels determined by the inflection point of the hydrodynamic size *versus* temperature curve using DLS was 38.3 °C [29], which is also in accordance with our previous studies on LCST of the equivalent OEGMA-based copolymers [16]. The produced nanogels were able to reversibly reduce their size, undertaking 70 % reduction in volume when the temperature rises above their VPTT [29]. Two mL of a SDS surfactant solution containing 0.035 mmol were added as nanogels stabilizer. All the components were dissolved in Milli-Q water with a final volume of 40 mL. The reaction mixture was purged with argon under stirring during 30 min, afterwards, the solution was heated to 70 °C, and the polymerization was initiated by the addition of KPS (2 mL, 0.037 mmol). The polymerization reaction was carried out during 6 h at 70 °C. The resulting BNC-nanogels were collected by repeated centrifugation at 10000 rpm for 10 min at 10 °C and washed with water. For the preparation of empty nanogels the protocol was identical to the previous one in absence of BNCs, except for the purification procedure. To recover empty drug-free nanogels after the synthesis it was necessary to ultracentrifugate them at 25000 rpm for 60 min at 15 °C (Beckman Coulter, Avanti J-20 XP equipped with JA25.50 rotor, USA). This process was required due to the small size and excellent stability of the nanogels in aqueous solution. Therefore, the separation of drug-loaded nanogels (that precipitate effectively at 10000 rpm) from empty nanogels is effective during BNC-nanogels centrifugation, as empty ones are removed in the supernatant during repeated washing cycles.

2.5. Synthesis of copper sulfide nanoparticles (CuS NPs)

CuS NPs were synthesized following the work of Ramadan *et al.* [31] with some modifications. Briefly, the synthesis was carried out in a 500 mL round flask by mixing 1.2 g of PVP K30 dissolved in 125 mL of DDI water with 500 μL of a 0.5 M solution of $CuCl_2$ and 125 mL of water with alkaline pH of 9. Afterwards, 32 μL of hydrazine solution was added under vigorous stirring, which gives place to the formation of Cu_2O seeds. One mL of Na_2S (320 mg/mL) was added to the previous dispersion while keeping it under heating at 70 °C for 2 h. Several washing cycles were performed by centrifugation at 10000 rpm, 10 min.

2.6. Synthesis of the nanohybrid CuS@BNC-nanogels

We decorated the nanogels with CuS NPs using electrostatic interactions. To obtain CuS NPs with high positive surface charge we functionalized them by the alternate electrostatic layer-by-layer (LbL) assembly technique with multilayers of biocompatible polyelectrolytes of opposite charge [32]. As the surface charge of initial CuS NPs is negative, first a layer of a positively charged polyelectrolyte PAH was introduced by adding a solution of CuS NPs (1 mg/mL) over a PAH solution of 2 mg/mL having ionic strength (6 mM NaCl). The solution was stirred during 3 h at room temperature and washed by centrifugation at 10000 rpm (10 min). After that, the positively charged CuS NPs (1 mg/mL) were incubated with PSS (2 mg/mL) in NaCl (6 mM). The negatively charged CuS NPs were finally coated with a layer of PAH to have a significant positive surface charge able to stabilize the NPs and couple them to nanogels through supramolecular electrostatic interactions.

To obtain the final vector composed of nanogels and NIR-sensitive CuS NPs the coupling was carried out through the electrostatic interactions of negatively charged nanogels and CuS NPs modified with multilayers of polyelectrolytes PAH/PSS/PAH to have a positively surface potential. To this aim, a dispersion of CuS NPs (1 mg/mL) were added dropwise over a solution of nanogels (5 mg/mL) under stirring. After 30 min the solution was centrifuged at 10000 rpm (12 min) to obtain the final nanomaterial named CuS@BNC-nanogels.

2.7. Light-triggered in vitro release experiments

In vitro drug release from CuS@BNC-nanogels was studied at body temperature (37 °C), below the volume phase transition (VPT) of nanogels at 38.3 °C [29]. The sustained release profiles were determined using 1 mL of 0.4 mg/mL dispersions in water using a thermoshaker (Biosan TS-100C, Riga, Latvia) set at 37 °C with mechanical agitation at 600 rpm. The dispersions were prepared to work under sink conditions below the drug saturation concentration according to the drug loading obtained. Three sam-

ples were taken for each release time point. The samples were centrifuged at 13000 rpm for 10 min and the supernatant was separated and filtered with a 0.22 μm syringe filter. The amount of bupivacaine released at each time point was calculated from the supernatant using GC–MS. The GC–MS samples were prepared by mixing 100 μL of the supernatant with 850 μL of ethanol and 50 μL of limonene solution in methanol as internal standard. To study the light-triggered release, 1 mL of CuS@BNC-nanogels (0.4 mg/mL) dispersed in water were exposed to several heating–cooling cycles using a collimated 808 nm laser diode at 5.2 W/cm^2 (such irradiance was used to obtain a fast response) and consisting on heating to 45 °C and then cool it down to body temperature (37 °C). After several heating–cooling cycles, the samples were centrifuged at 13000 rpm for 10 min and the supernatant was separated and filtered with a 0.22 μm syringe filter to determine bupivacaine concentration using GC–MS.

Drug loading (DL%) was quantified using the direct method by the extraction of the drug using ethanol. The drug loading was calculated by means of the following formula:

$$\text{Drug loading}\%(\text{DL}\%) = \frac{\textit{Mass of drug in nanoparticles}}{\textit{Total mass of nanoparticles}} \text{x}100$$

2.8. Nanomaterials characterization

The drug content of CuS@BNC-nanogels was determined using a Gas Chromatograph-Mass Spectrometer (GC–MS QP2010 SE, Shimadzu, Kyoto, Japan), equipped with an AOC-20i auto injector. The mass spectrometer was set at an interface temperature of 280 °C, an ion source temperature of 200 °C, with a mass range of 35 to 300 *m*/*z* and a solvent cut time of 2.5 min. The capillary column used to separate the compounds was a Zebron™ ZB-50 (Phenomenex, USA) having dimensions 30 m (length) × 0.25 mm (diameter) × 0.25 μm (film thickness). The injector temperature was adjusted at 250 °C and the split mode was used at a 10:1 ratio. The GC oven temperature was initially set at 50 °C and further increased to 170 °C using a ramp rate of 30 °C/min, then raised at 45 °C/min to 250 °C (0.5 min hold) and finally raised at 10 °C/min to 300 °C, and hold for 1.5 min. The carrier gas used was helium (>99.999%) with a flow linear velocity of 31 cm/s. The system was programed with 11 mL/min of total flow rate and 0.73 mL/min of column flow. Bupivacaine was identified by its retention time (RT) and mass fragmentation pattern. Bupivacaine was quantified by the peak area comparison relative to the limonene used as internal standard. The data peak processing was carried out by means of Shimadzu' GC–MS solution software.

UV–vis spectra were recorded using a Jasco V670 spectrophotometer to evaluate the characteristic CuS surface plasmon resonance band in the NIR region of the selectromagnetic spectrum.

Zeta potential was used to analyze the surface charge during the LbL polyelectrolyte deposition on the surface of CuS NPs. Zeta potential of the colloidal suspensions was performed on a Brookhaven 90Plus particle size analyzer using the ZetaPALS software in 1 mM KCl aqueous solution at a pH = 6 and 25 ± 0.1 °C. The zeta potential was determined by studying their electrophoretic mobility and then applying the Smoluchowski equation.

Thermogravimetric analysis allowed to determine the organic and inorganic contend of the nanocomposite. TGA (Mettler Toledo TGA/STDA 851e) was carried out in a temperature range between 30 and 800 °C using a heating rate of 10 °C/min, under nitrogen atmosphere with a flow rate of 50 mL/min.

X-ray diffraction (XRD) was used to assess the crystallinity of BNCs and to corroborate the inclusion of the nanocrystals in the final nanocomposite. The diffractograms were recorded in a Philips X-Pert diffractometer with a monochromatized Cu Kα radiation source (λ = 1.54060 Å, 40 kV, 20 mA) in 2Θ ranging from 5° to 60° with a step of 0.013 and 5 s of analysis time.

Copper content in the resulting CuS@BNC-nanogels was determined using Microwave Plasma-Atomic Emission Spectrometry (MP-AES 4100, Agilent, CA, USA). MP-AES is equipped with an Inert OneNeb nebulizer and a double-pass glass cyclonic spray chamber. Nitrogen gas was obtained from a generator connected to an air compressor. Instrumental parameters such as the nebulizer gas pressure, the viewing position (i.e., the analytical observation zone in the plasma), and the background correction were optimized automatically using the instrument software. The acid digestion method was used for the preparation of samples. Three replicates were performed setting 3 s of read time and 15 s for torch stabilization time.

Transmission electron microscopy (TEM) images were recorded in a T20-FEI Tecnai thermoionic microscope operated at an acceleration voltage of 200 kV. Samples were dropped in carbon coated copper grids, dried at room temperature and stained with a negative staining agent (3% phosphotungstic acid) when necessary to improve the contrast of the polymeric nanogels. TEM images were analyzed using the open source image processing software ImageJ to obtain size distributions of nanoparticles. Scanning-transmission imaging with a high-angle annular dark-field detector (HAADF- STEM) and energy-dispersive X-ray spectroscopy (EDS) analysis were carried out in a scanning transmission electron microscope (STEM; FEI Tecnai F30, operating at 300 kV).

Fourier transform infrared (FTIR) spectroscopy analysis was performed on a Bruker Vertex 70 FTIR spectrometer equipped with a deuterated triglycine sulfate (DTGS) detector and a Golden Gate diamond attenuated total reflectance (ATR) accessory. Data points were collected at a resolution of 4 cm^{-1} from the 4000–600 cm^{-1} wavelength range and 80 number of scans.

Nanoparticle irradiation was performed using a 808 nm-laser diode (model MDL-III-808–2 W, Changchun New Industries Optoelectronics Technology Co., Ltd., Changchun, P.R. China). Samples were irradiated as dispersions in water at a concentration of 0.4 mg/mL using a laser irradiance of 5.2 W/cm^2. The temperature variations were registered using a thermocouple.

2.9. Cytocompatibility analysis

The cytocompatibility of CuS@BNC-nanogels, CuS@nanogels and bupivacaine hydrochloride was *in vitro* evaluated in four cell lines in order to explore the potential clinical use of the synthesized bupivacaine loaded nanosystems for pain relief.

Human dermal fibroblasts (Lonza, Belgium), human glioblastoma cells (U251MG; kindly gifted by Dr. Pilar Martín-Duque), mouse mesenchymal stem cells (mMSC; donated by Dr. Pilar Martín-Duque) and THP1 cells (American Type Culture Collection, USA) were the cell lines assayed. Human dermal fibroblasts and U251MG cells were grown in Dulbecco's modified Eagle's medium (DMEM) high glucose containing stable glutamine (Biowest, France) and supplemented with fetal bovine serum (FBS, 10% (v/v), Thermo Fisher Scientific, MA) and antibiotic–antimycotic (60 μg/mL penicillin, 100 μg/mL streptomycin, and 0.25 μg/mL amphotericin B; Biowest, France). mMSCs were cultured in DMEM-F12 (Biowest, France) supplemented in the same way as described above for DMEM high glucose. THP1 cells were grown in RPMI 1640 containing stable glutamine (Biowest, France) and supplemented with 10% v/v FBS (Thermo Fisher Scientific, MA), 1% HEPES, 0.1% 2-mercaptoethanol 50 mM, 1% non-essential amino acids, 1% sodium pyruvate 100 mM and antibiotic–antimycotic (60 μg/mL penicillin, 100 μg/mL streptomycin, and 0.25 μg/mL amphotericin B; Biowest, France). *In vitro* differentiation of THP1 cells to macrophages was carried out by adding 1 μM phorbol 12-myristate 13-acetate (Sigma Aldrich, USA) to the cell culture

medium for 72 h. All cell lines were cultured under humidified atmosphere containing 5% CO_2 at 37 °C except for mMSCs which were cultured under hypoxia (3% O_2).

The Blue Cell Viability assay (Abnova, Taiwan) was performed to determine the *in vitro* cytotoxicity of CuS@BNC-nanogels, CuS@-nanogels and bupivacaine hydrochloride at different concentrations in the range of 0.01–0.5 mg/mL except for bupivacaine hydrochloride that was tested at the equivalent loaded concentrations (0.006–0.293 mg/mL). Human dermal fibroblasts (6000 cells/well), U251MG cells (5000 cells/well), mMSCs (5000 cells/well) and THP1 macrophages (70000 cells/well) were seeded in 96-well plates and incubated with the tested compounds for 24 h. Then, the reagent was added (10% v/v) and incubated for 4 h. The fluorescence was read at excitation and emission wavelengths of 530 and 590 nm, respectively (Synergy HT microplate reader, Biotek, USA). The potential of the compounds interference with the methodology was tested and discarded. Cell viability was calculated as a relative percentage of the untreated control-cells value. The percentages obtained represent the average of five experiments.

Moreover, flow cytometry assays were carried out to evaluate the potential effects in cell cultures of the treatment with CuS@BNC-nanogels, CuS@nanogels and bupivacaine hydrochloride. Human dermal fibroblasts, U251MG cells, mMSCs and THP1 macrophages were incubated for 24 h with the tested compounds at a subcytotoxic concentration determined in the Blue Cell Viability assay. Then, samples were collected and analyzed by flow cytometry to study cell apoptosis and cell cycle. Apoptosis was assessed by adding annexin-binding buffer to the cell pellet. Next, cell suspensions were stained for 15 min with annexin V-FITC and propidium iodide to be further analyzed by flow cytometry after incubation with annexin-binding buffer. The percentages of cell viability, early apoptosis, late apoptosis and necrosis were determined by a FACSARIA BD equipment and the FACSDIVA BD software (BD, USA). On the other hand, cell cycle was analyzed through fixing the samples with ethanol (70%) and staining the DNA by adding RNase A and propidium iodide. The distribution of cell cycle phases was determined in a FACSARRAY BD equipment with the MODIFIT 3.0 Verity software (BD, USA). Control samples were also run in both flow cytometry methodologies to determine cell basal status.

2.10. Statistical analyses

Data are reported as mean ± SD. Normal distribution of the variables was analyzed by the Shapiro-Wilk test followed by the U-Mann-Whitney or Student test (StataSE 12 statistical software, StataCorp LP, USA). Statistically significant differences among groups were considered when $p \leq 0.05$.

3. Results and discussion

3.1. Characterization of CuS@BNC-nanogels

CuS@nanogels loaded with BNCs were prepared by electrostatic coupling of negatively charged BNC-nanogels [29] and positive surface charged CuS NPs modified by LbL assembly technique with alternate multilayers of polyelectrolytes of opposite charge (Scheme 1). The zeta potential of BNC-nanogels, synthesized using the aqueous precipitation polymerization method described in our previous work [29], was − 10.47 ± 0.33 mV. This negative surface charge is provided by the SDS surfactant used in the stabilization of the nanogels [33]. The obtained CuS NPs showed a negative zeta potential of −17.48 ± 0.83 mV, that was reverted by its functionalization with alternate layers of PAH/PSS/PAH. The changes in the zeta potential during LbL coating of CuS NPs via alternate adsorption of PAH and PSS polyelectrolytes are depicted in Fig. 1a. The resulting polyelectrolyte coated CuS NPs exhibited a positive surface charge of + 22.8 ± 0.47 mV. This positive surface potential rendered an effective electrostatic coupling with the negatively charged BNC-nanogels, generating a final vector with zeta potential of − 7.35 ± 0.22 mV at neutral pH.

UV–vis spectroscopy was employed to characterize the surface plasmon resonance-induced absorption band characteristic of CuS NPs. The UV–Vis spectra of CuS@BNC-nanogels presented the broad absorption band in the NIR region of the spectrum, in the same way as CuS NPs functionalized with polyelectrolytes (Fig. 1b). The preservation of this characteristic absorption in the NIR region allows the activation of CuS@BNC-nanogels upon irradiation in order to trigger the release of the associated drug. TEM characterization of CuS@BNC-nanogels (Fig. 1c-d) showed that the nanogels were effectively decorated with the CuS NPs on their surface. According to TEM images, BNC-nanogels of a mean size of 148 ± 35 nm [29] were grafted to CuS NPs of 108 ± 25 nm (Fig. S1). Fig. S2 shows illustrative TEM images of BNCs of 22 ± 7 nm obtained by the anti-solvent precipitation method described above. The multilayer coating of CuS NPs produced by the adsorption of PAH and PSS polyelectrolytes is perceived in the TEM images after sample staining with phosphotungstic acid [34]. The halo around the nanoparticles corresponds to the tungsten-containing PAH and PSS grafted on their surfaces. As a result, CuS NPs present a grey organic layer with a thickness of 6 ± 2 nm around the surface of CuS NPs. Inset in Fig. 1d represents a detailed HAADF-STEM image of a CuS nanoparticle. In Fig. 1e-f, HAADF-STEM images showed a sample of CuS@BNC-nanogels to identify the location of Cu and S atoms by Z–contrast, and the corresponding EDS spectra (Fig. 1e). CuS NPs are hollow structures due to the Kirkendall diffusion effect, where sulfur diffuses into the Cu_2O template particles at the same time that copper diffuses outwards [35]. Fig. 1f shows the Cu and S EDS profiles of a representative CuS NP, where the red line depicts the spatial localization of the EDS profile. This EDS profile shows higher concentration of Cu and S in the shell (corresponding to the particle walls), and lower concentration in the core, confirming the hollow structure. Empty nanogels were also coupled to CuS NPs for the sake of comparison. The zeta potential obtained for empty nanogels was − 6.7 ± 0.9 mV, close to the one of drug loaded nanogels. Fig. 1g-h report a typical sample of the coupling of empty nanogels, which exhibited a size of 64.7 ± 8.6 nm [29], to the positively charged CuS NPs functionalized with polyelectrolytes. The smaller size of empty nanogels produced a different disposition around the CuS NPs, allowing the attachment of a higher number of nanogel-based particles on the surface. When the nanogels are loaded with BNCs their size becomes larger than the one of CuS NPs, thus the attachment of several nanogels around CuS NPs is sterically hindered, and a lower number of gel-based particles are coupled per CuS NPs. This disposition could be effective for the photothermal heating activation of CuS NPs by NIR-light irradiation, transmitting efficiently the heat necessary to trigger the thermo-responsiveness of the nanogels by direct close transference of heat between coupled CuS NPs and nanogels.

XRD is usually applied to study the crystalline structure of drugs as well as to collect evidences of drug encapsulation. The results of XRD (Fig. 2a) show that the CuS@BNC-nanogels exhibited intense diffraction peaks at 10°, 16.2°, 17.8°, 20°, 21.5°, 23.8° and 25.5°, indicating the presence of the drug crystalline structure in BNCs (Fig. S3). The drug remains in a well-crystallized state into the nanocomposite. Empty-nanogels showed no diffraction peaks in the spectrum, presenting the typical diffractograms of amorphous compounds (Fig. S3). CuS NPs functionalized with PAH/PSS/PAH show intense diffraction peaks at 29.3°, 32° and 48° cor-

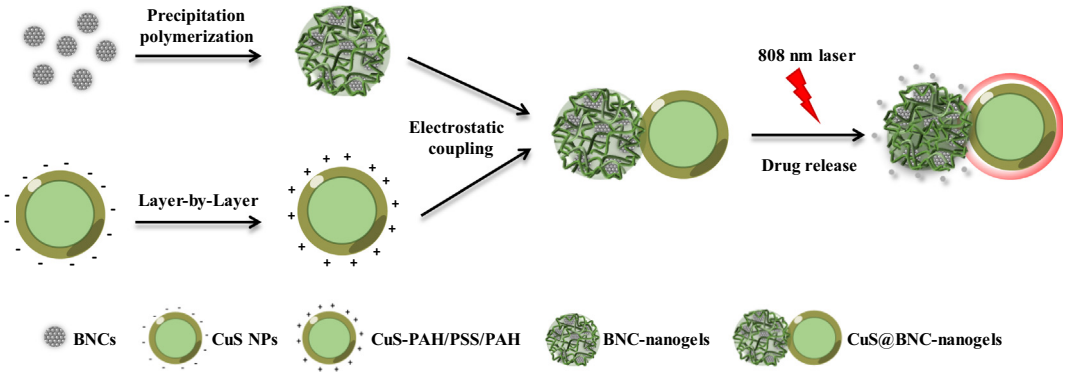

Scheme 1. Schematic illustration of the main synthesis procedures and photothermal activation of CuS@BNC-nanogels.

responding to the characteristic diffraction planes of covellite phase that shows maximum absorption in the NIR region [35]. FTIR spectroscopy is a useful tool for nanomaterials characterization that allows to determine the constituting elements and their bonding arrangement. Fig. 2b shows the spectrum of CuS@BNC-nanogels as well as the spectra of the main components in the nanomaterial, CuS NPs PAH/PSS/PAH, BNC-nanogels and BNCs. The infrared spectrum of CuS@BNC-nanogels shows the distinctive bands of BNCs and BNC-nanogels. The characteristic signals of the BNCs can be identified at 3200 cm^{-1} cosigned to stretching of hydrogen-bonded N—H group of the mono-substituted amides (O=C—N—H), around 2927 cm^{-1} attributed to C—H stretching vibrations, the peaks at 1700–1600 cm^{-1} assigned to C=C and C=O stretching, at 1680–1630 cm^{-1} to amide carbonyl stretching band, at 1550 cm^{-1} to C—N stretching vibrations together with N—H bending and at 1250 cm^{-1} to C—N—H stretch vibrations [36]. The peak appeared around 1720 cm^{-1} was ascribed to the stretching vibrations of C=O groups in the P(MEO2MA-*co*-OEGMA500) polymer [16]. Distinctive CuS NPs absorption bands are shown in CuS@BNC-nanogels spectra, corresponding to the R-SO_3^- group of PSS at 1190–1009 cm^{-1} [37] and the band at 618 cm^{-1} indicating the existence of Cu-O bonds [38]. Thus, FTIR results are indicative of the presence of BNCs and CuS NPs in the final vector, in agreement with results obtained in our previous analysis. Altogether, XRD and FTIR analysis endorsed the incorporation of a high quantity of BNCs into CuS NPs@ nanogels.

The composition of CuS@BNC-nanogels was studied using TGA, MP-AES and GC–MS to determine the drug content. TGA curves of BNC-nanogels (Fig. S4a) presented two weight loss at 225 °C and 340 °C attributed to the thermal decomposition of bupivacaine and P(MEO_2MA-*co*-$OEGMA_{500}$), respectively [25]. Otherwise, the TGA analysis of CuS NPs coated with PAH/PSS/PAH (Fig. S4b) showed a first weight loss up to 100 °C ascribed to the loss of water molecules linked to PAH/PSS/PAH polymers and a second loss between 200 and 400 °C attributed to the polymers thermal decomposition. The remaining material from 400 °C corresponds to CuS. The thermal decomposition curves of CuS@BNC-nanogels are depicted in Fig. 2c. CuS@BNC-nanogels exhibit two differentiated weight losses. The first around 150–260 °C was ascribed to the bupivacaine thermal decomposition. The second weight loss occurred at around 260–420 °C and was attributed to the degradation of the polymers [25]. There was no evidence of weight loss after 400 °C, and this remaining material after complete degradation of organic compounds was ascribed to the remaining inorganic CuS. Therefore, the CuS content corresponded to 17 wt% of the final nanomaterial, so that the other 83 wt% of the nanocomposite was assigned to the organic material comprising BNCs and polymers. Taking into account the weight loss ranges of the individual components, the weight loss up to 260 °C attributed to the bupivacaine content in the final nanomaterial corresponded to 63 wt%. This high drug loading was verified by GC–MS analysis, as the overlapping in the weight loss curves of the different organic components could contribute to a low accuracy in the drug determination when using TGA. The drug loading of CuS@BNC-nanogels measured using GC–MS was 65.5 ± 5.9 wt%. The Cu content in CuS@BNC-nanogels was also quantified using MP-AES in order to determine the real amount of Cu contained into the final material. The MP-AES analysis revealed a Cu content in the nanomaterial of 9.6 ± 1.2 wt%. The results are in fair agreement with the estimation of 17 wt% CuS content obtained by the TGA analysis. TGA, MP-AES and GC–MS results showed that the final CuS@BNC-nanogels hold an elevated drug content useful for their application in pain relief.

3.2. Light-responsive drug release profile

In previous studies, CuS NPs were used for effective photothermal heating under NIR illumination [35]. Furthermore, photothermal properties of NIR-responsive nanoparticles have been extensively used in photothermal cancer therapy using different nanomaterials such as gold nanoparticles [39], gold nanorods [40] and nanoplatforms integrating nanomaterials and functional polymers [41]. In order to investigate the thermoresponsive drug delivery profile of CuS@BNC-nanogels the first step was to examine the photothermal properties of the nanomaterial upon 808 nm NIR irradiation. Fig. 2d depicted the photothermal response of 1 mg/mL CuS@BNC-nanogels dispersions depending on the irradiance supplied. The photothermal heating curves obtained at irradiances between 1.4 and 5.2 W/cm^2 indicated an increase in the heating rate proportional to the increment of the irradiance supplied. As shown in Fig. 2d, the temperature of the CuS@BNC-nanogels solutions increased by 1.2 °C/min (curve 1.4 W/cm^2, from 27 to 37.5 °C over 8.6 min). When the power density was increased to 2.8 W/cm^2 the temperature increased by 2.6 °C/min (from 27 to 48 °C over 8 min). An irradiance of 3.5 W/cm^2 increased the solution temperature by 5.2 °C/min (from 28.8 to 55.2 °C over 5.1 min). Finally, the irradiance of 5.2 W/cm^2 increased the solution temperature by 8.2 °C/min (from 27 to 60 °C over 4 min). Applying 5.2 W/cm^2, the CuS@BNC-nanogels generated a ΔT of 33 °C in 4 min. Providing this NIR power density it is possible to heat from physiological temperature (37 °C) to 45 °C in 1.5 min, producing the rapid collapse of the nanogels, thus such irradiance was used to obtain a fast response. The irradiation of a water solution used as control assay exhibited only a slight increase in temperature (Fig. S5).

Results of the *in vitro* release experiments are shown in Fig. 2e. The release profile of CuS@BNC-nanogels at 0.4 mg/mL, concentration way below the drug saturation taking into account the loading of 65.5 wt%, is shown at 37 °C. The drug encapsulated was completely released after 24 h at physiological temperature, presenting

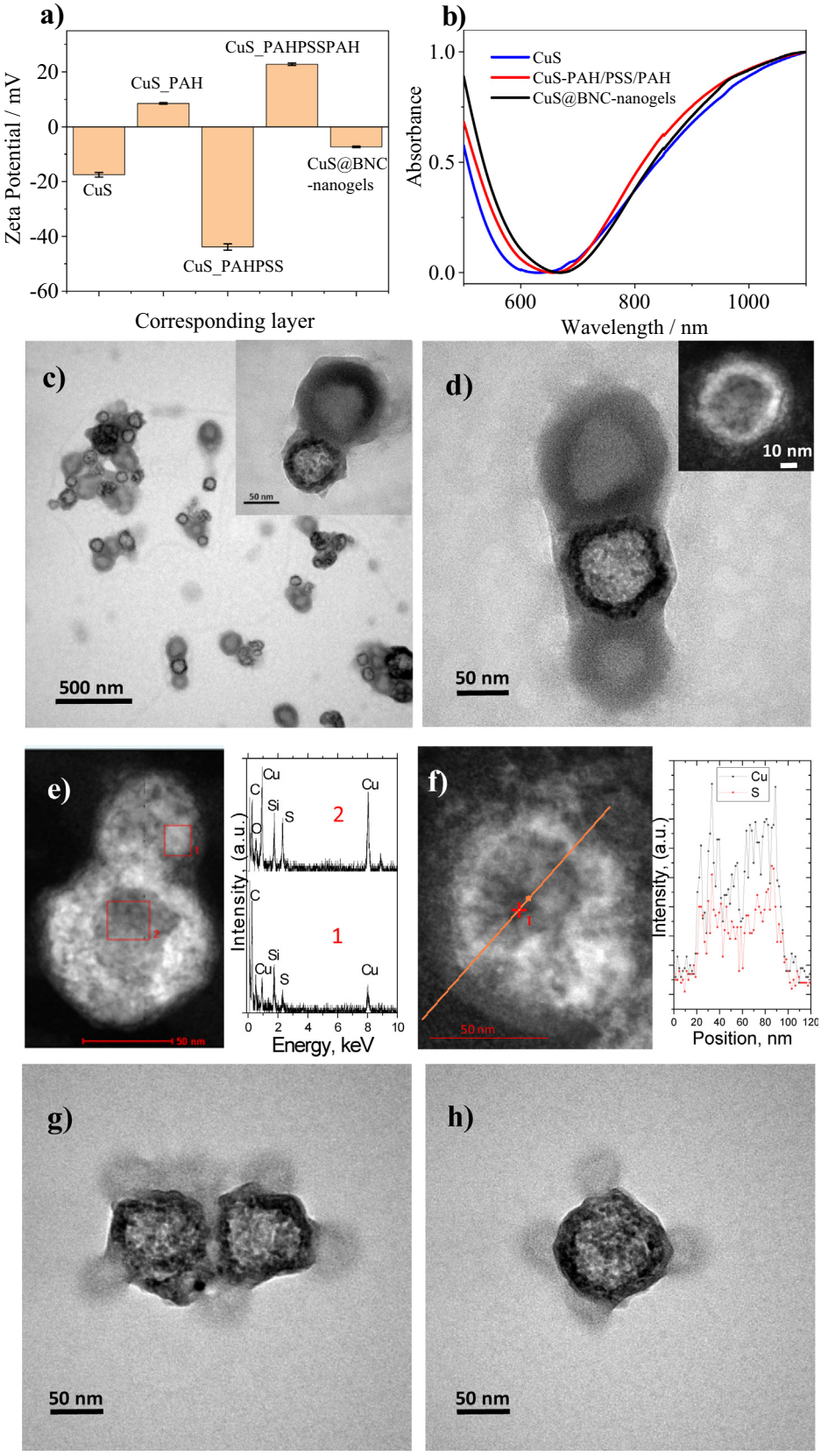

Fig. 1. (a) Zeta potential during CuS NPs LbL coating via alternate adsorption of polyelectrolytes and coupling to BNC-nanogels. (b) UV–Vis spectra of CuS, CuS-PAH/PSS/PAH and CuS@BNC-nanogels. Representative TEM image of (c-d) CuS@BNC-nanogels. Inset in (c) depicts a detailed HAADF-STEM image of a CuS nanoparticle. (e) HAADF-STEM image and EDS spectra of CuS nanoparticles (f) HAADF-STEM image and Cu/S EDS profiles of a representative CuS nanoparticle. The red line in the image depicts the spatial localization of the EDS profile. (g-h) TEM images of empty CuS@nanogels.

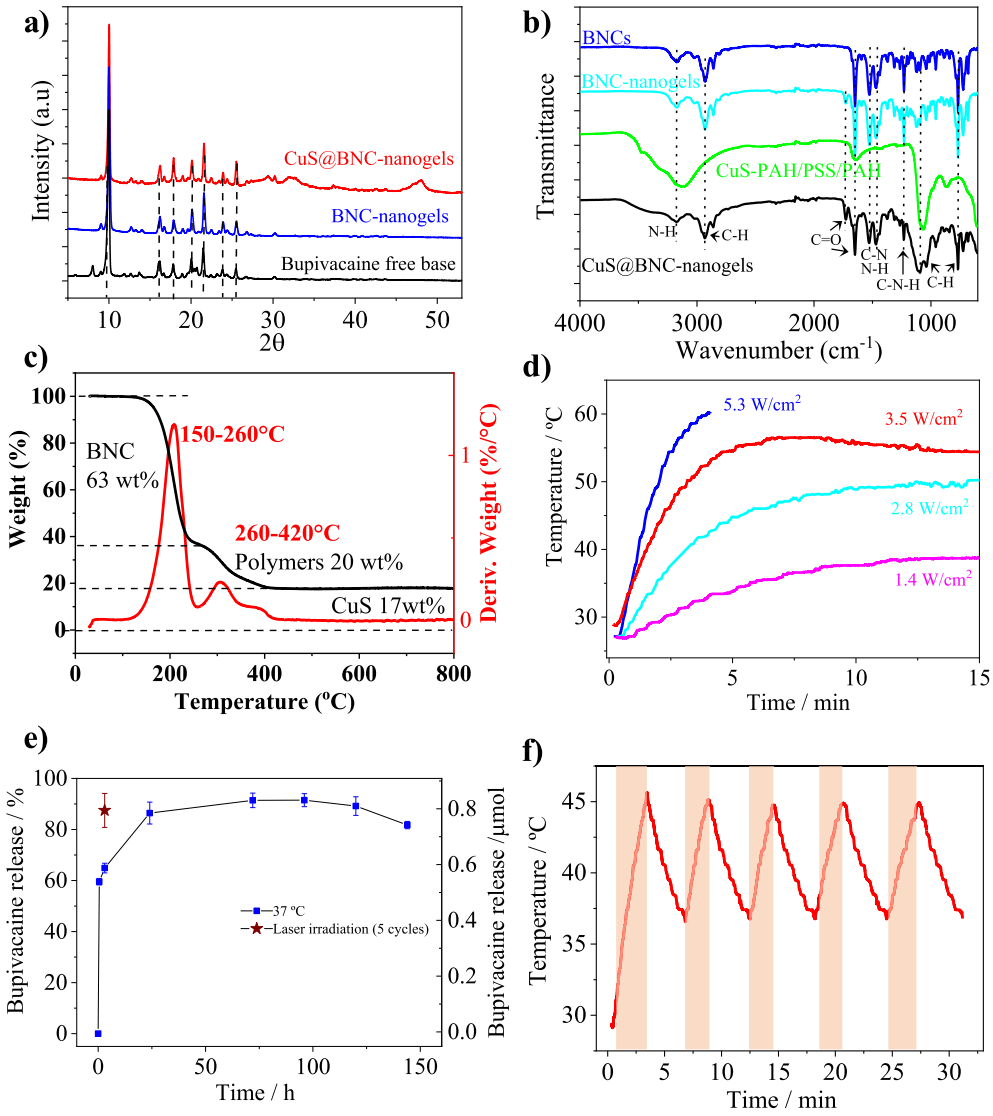

Fig. 2. (a) XRD diffractograms of CuS@BNC-nanogels, BNC-nanogels and bupivacaine free base. (b) FTIR spectra of CuS@BNC-nanogels, CuS-PAH/PSS/PAH, BNC-nanogels and BNCs. Labels point out several functional groups present in the nanomaterials. (c) TGA (black) and derivative of TGA (red) plots for CuS@BNC-nanogels. (d) Heating curves of CuS@BNC-nanogels at different irradiances ranging from 1.4 to 5.2 W/cm^2. (e) Bupivacaine release profiles from CuS@BNC-nanogels at 37 °C. After 3 h of release at 37 °C, 5 pulses of irradiation were applied from 37 to 45 °C using laser irradiation at 808 nm and 5.2 W/cm^2 (represented as a star). Data are means ± SD (N = 3). (f) Heating cycles of CuS@BNC-nanogels (0.4 mg/mL) under laser irradiation at 808 nm; 5.2 W/cm^2.

a burst release in the initial half an hour, probably due to the fraction of NCs attached in the outer region of the nanogels. After that, a slower release event occurs that reached an equilibrated drug release after 24 h. The 65 wt% of the drug was released after 3 h (0.42 mg of bupivacaine per mg of nanomaterial), and at this 3 h time point the release of the remaining drug was promoted by the irradiation with 808 nm laser to demonstrate that it is possible to activate an additional drug dose on-demand when required. The photothermal stimulus was applied to trigger the release by irradiation with five laser on/off cycles. The samples were irradiated with the 808 nm laser for 2 min (laser-on), to heat up from 37 °C to 45 °C. Subsequently, the laser was switch off and the solution cooled down to 37 °C for 3.5 min (laser-off). The cycles between 37 and 45 °C produce the transition of the nanogels above their VPT of 38.3 °C [29], triggering the release of additional drug. When the temperature of nanogels is lower than the VPTT, water molecules align around the hydrophilic moieties of the polymer. However, at temperatures above the transition temperature, owing to the hydrophobicity of the surrounding groups, water molecules start detaching, with a consequent phase separation between the water and polymer. Consequently, as the temperature increases hydrophobic-hydrophobic interactions become more important than hydrophilic-hydrophilic interactions, which eventually leads to aggregation of hydrophobic moieties, reduction in the nanogel volume and subsequent drug release. The reversible phase separation produces the desorption not only of the water molecules interacting with the polymer, but also of drug molecules confined in the nanogel structure that are expelled to the medium. As an example, Cazares-Cortes *et al.* [42] prepared thermosensitive OEGMA-based nanogels for the remote release of DOX triggered by magnetic nanoparticles. It was demonstrated that DOX release from the nanogels was driven by the application of a magnetic field that generated heat due to the interaction with magnetic nanoparticles acting as the driving force for drug release. As shown in Fig. 2f, no significant variation was observed in photothermal heating during the five cycles indicating a photothermal stability of CuS@BNC-nanogels under five consecutively repeated cycles using NIR illumination. The analysis of the drug released after the NIR activation

(represented as a star) showed that approximately, after five laser on/off cycles, the remaining 30 wt% of the drug encapsulated was released (obtaining the release of 0.57 mg of bupivacaine per mg of nanomaterial). Thus, when the photothermal stimulus was applied a triggered on-demand release at a specific time point can be accomplished to provide an additional anesthetic effect when needed by using CuS@BNC-nanogels. Therefore, the photothermal-induced nanogel transition can be used to provide a thermo-responsive triggered release of local anesthetics for pain relief in real applications.

To our knowledge, this is the first report in the literature describing the use of CuS NPs attached to P(MEO_2MA-*co*-$OEGMA_{500}$) nanogels for the fabrication of a remotely photothermal-activated pulsed device for the supply of local anesthetics. Also, the encapsulation of anesthetics in the form of nanocrystals has not been previously reported in on-demand photo-responsive nanocarriers. A few studies have described the use of hybrid nanomaterials for on-demand photothermal-release of anesthetics with on–off switching ability [43]. Kohane *et al.* [44] reported the preparation of a phototriggerable formulation consisting on gold nanorods (GNRs) attached to the membrane of drug-containing liposomes. The photothermal properties of GNRs enabled the fast transition of lipid bilayers and the subsequent drug release. This formulation containing the anesthetic tetrodotoxin (TTX) loaded into the liposomes was tested *in vivo,* showing that NIR-light irradiation successfully produced on-demand control of local anesthesia, furthermore with a very reduced toxicity. However, the loading capacity of this liposome-based formulation was 0.3 wt% of TTX, far from the drug loading value obtained in our work using the nano-crystallized drug (65.5 wt%), thus an increase in the drug loading could improve its performance despite of the superior anesthetic effect of TTX over bupivacaine at the same dose. Previous works encapsulating bupivacaine hydrochloride into thermoresponsive polymeric microparticles for phototriggered local anesthesia reached a maximum DL% of 11 wt% [23]. Other hybrid core–shell nanoparticles achieved values of 2–3 wt % of bupivacaine hydrochloride loadings [15,25]. Hence, the incorporation of nano-crystallized drugs into nanostructures could significantly propel the relevance of on-demand delivery systems for many biomedical applications.

3.3. In vitro cytocompatibility

In vitro cytotoxicity and potential effects in cell apoptosis and cycle of the treatment for 24 h with CuS@BNC-nanogels, CuS@-nanogels and bupivacaine hydrochloride were evaluated in four different cell lines (mMSCs, U251MG, human dermal fibroblasts and human macrophages). This battery of different cell lines was selected to cover a wide range of cell lines including somatic, multipotent stromal cells and even tumor-derived cell lines.

Fig. 3 displays the results obtained from the cytotoxicity assays. Nanogels (Fig. 3a and b) showed a dose-dependent cytotoxicity exerting a similar trend in the four cell lines assayed though not loaded nanogels (Fig. 3b) exhibited barely lower viability than the loaded ones (Fig. 3a). This is attributed to the higher CuS content in the CuS@nanogel constructs compared to the total mass of those carriers in comparison with the proportional lower amount of CuS in CuS@BNC-nanogels. mMSCs were less affected by the addition of nanogels showing slightly higher viability percentages than the other cell types whereas macrophages appeared to be more affected at the intermediate concentrations tested (0.02–0.1 mg/mL) probably due to their phagocytic nature [45,46]. However, bupivacaine hydrochloride exhibited lower toxicity at the corresponding loaded concentrations (0.006–0.293 mg/mL) showing again the same trend regarding the higher viability of mMSCs and lower viability of macrophages but only at the highest concen-

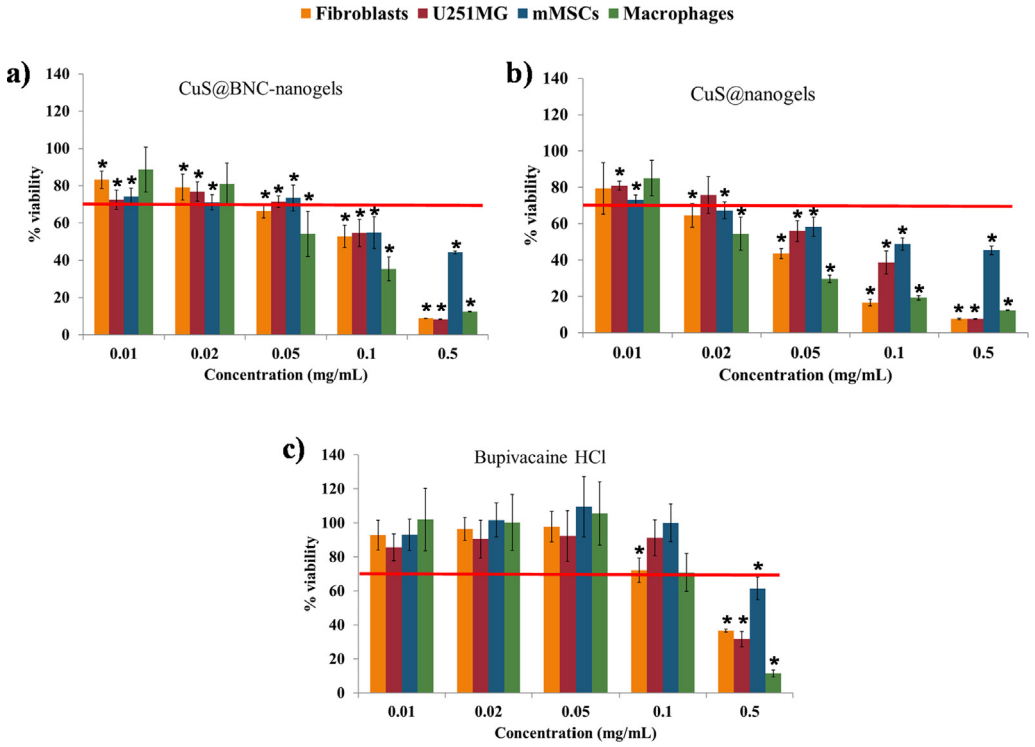

Fig. 3. Cell viability of CuS@BNC-nanogels, CuS@nanogels and bupivacaine hydrochloride in the four cell lines assayed after 24 h. Bupivacaine hydrochloride concentration corresponds to that loaded in CuS@BNC-nanogels (0.006–0.293 mg/mL). The red line depicts the threshold of 70% of cell viability in accordance with ISO 10993–5 [47]. Percentages are displayed as mean ± SD (N = 5). Statistical analyses refer to control samples (untreated cells) that exerted 100% viability. Statistically significant differences among groups were considered when $p \leq 0.05$.

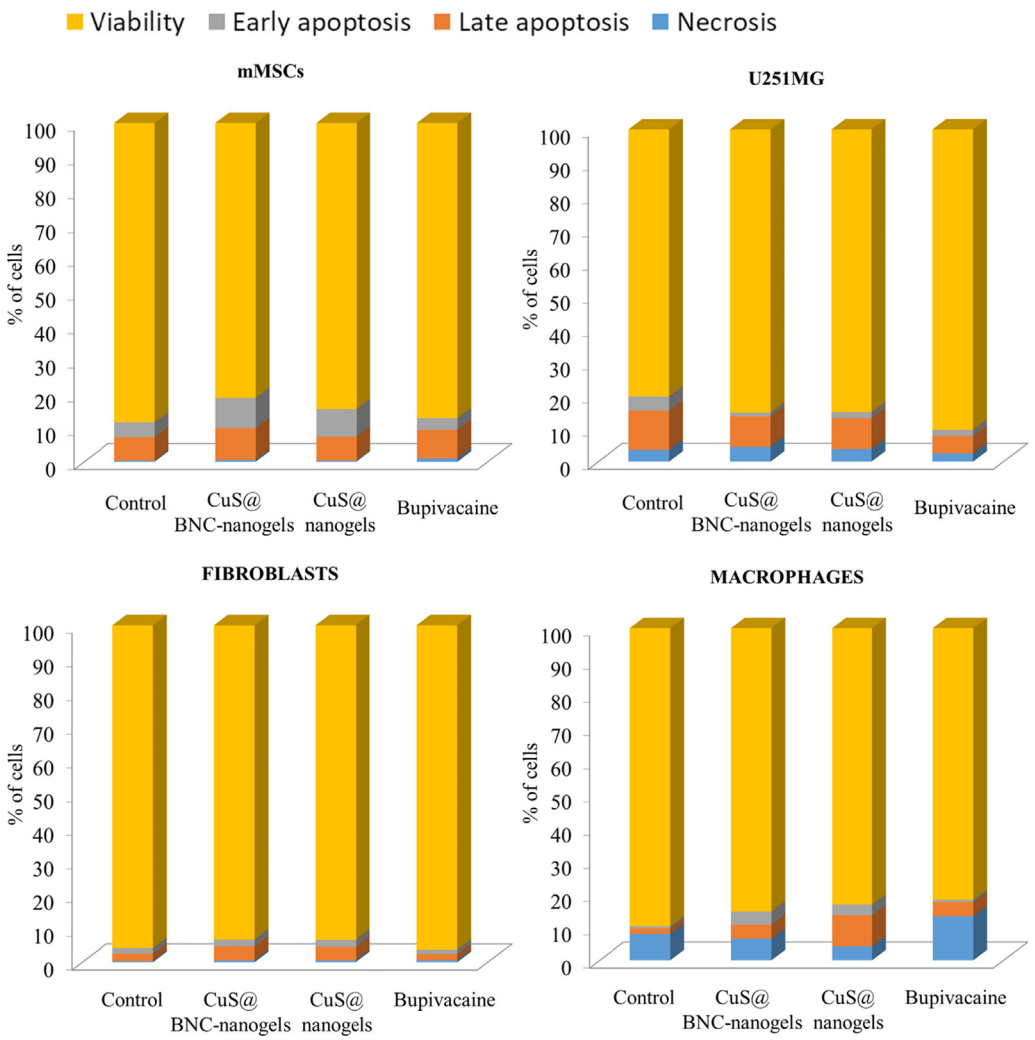

Fig. 4. Percentages of both early and late apoptotic, alive and necrotic cells after treatment with CuS@BNC-nanogels (0.05 mg/mL), CuS@nanogels (0.02 mg/mL) and bupivacaine hydrochloride (at equivalent concentration to that loaded in CuS@BNC-nanogels at 0.05 mg/mL) for 24 h.

trations assayed (0.1 and 0.5 mg/mL corresponding to the loaded concentrations of 0.059 and 0.293 mg/mL, respectively). These data are in agreement with our previous studies regarding cell treatment with CuS NPs [15,35] and free bupivacaine [15,24] even though CuS@BNC-nanogels and CuS@nanogels displayed a slightly higher toxicity than the nanocomposites based on amine terminated P(MEO_2MA-*co*-OEGMA) grafted on the surface of CuS NPs [15], probably owing to the different synthesis procedures. Considering these results and the recommendations of the ISO 10993–5 standard [47] which determines a threshold of 70% viability to establish the subcytotoxic concentration, flow cytometry experiments were carried out at 0.05 mg/mL for CuS@BNC-nanogels and 0.02 mg/mL for CuS@nanogels whereas 0.05 mg/mL (0.03 mg/mL of loaded bupivacaine hydrochloride) was chosen as the subcytotoxic concentration for the free anesthetic according to that loaded in CuS@BNC-nanogels.

Flow cytometry studies were developed to elucidate the potential effects of cell treatment with CuS@BNC-nanogels, CuS@-nanogels and bupivacaine hydrochloride concerning cell membrane or apoptosis and cell cycle (Fig 4.Fig 5. and S6). Fig 4. and S6 depict the percentages of viability, apoptosis (early and late) and necrosis obtained from cell samples incubated with the tested compounds at subcytotoxic doses for 24 h. Compared to the control samples, the treatment with both nanogels and bupivacaine hydrochloride did not exert significant changes, only a slight increase (<10%) of apoptosis (early + late) in macrophages, but showing percentages close to those obtained from non-treated cells (control sample). In this line, Fig 5. and S6 show the results of the distribution of cell cycle phases in which it can be observed that only fibroblasts showed slight changes in the distribution of G1, S and G2 (<18%), being the other percentages very close to those displayed by non-treated cells (control sample). These results are in accordance with our previous studies referring to the non-detrimental effects after cell treatment with CuS NPs, OEGMA-based thermoresponsive nanogels and bupivacaine [15,24,35]. Considering these results, the cytocompatibility of the synthesized nanogels has been clearly demonstrated at the doses tested in four cell lines for their future potential biomedical application.

4. Conclusions

In this study, we have successfully developed thermosensitive NIR light-responsive nanomaterials loaded with nanocrystals of the anesthetic drug bupivacaine. The incorporation of CuS NPs to the thermoresponsive nanogels provided their photothermal ability which allowed a phototriggered release of the local anesthetic modulated by NIR irradiation. The release studies showed that

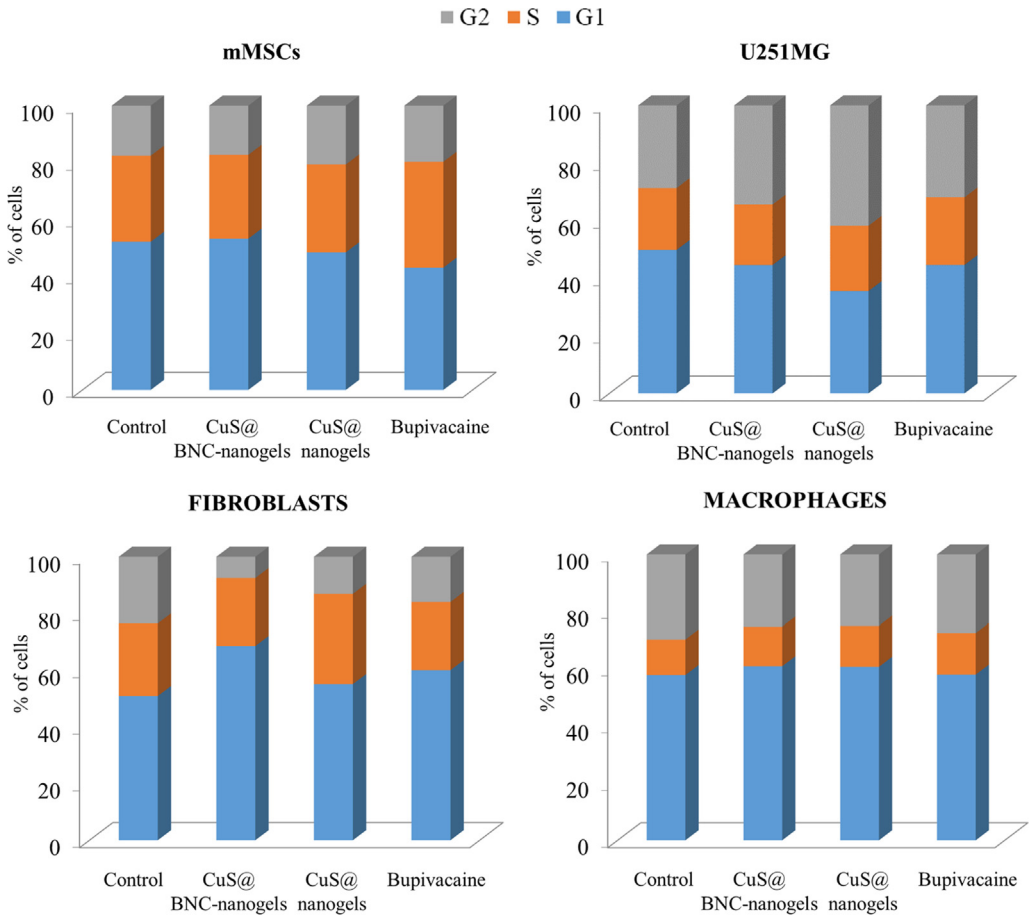

Fig. 5. Cell cycle population distribution (percentage of cells, %) after treatment with CuS@BNC-nanogels (0.05 mg/mL), CuS@nanogels (0.02 mg/mL) and bupivacaine hydrochloride (at equivalent concentration to that loaded in 0.05 mg/mL CuS@BNC-nanogels) for 24 h.

the dose of drug administrated could be modified by NIR irradiation. The excellent drug loading content achieved by the encapsulation of the drug in a nano-crystalized form confirmed the suitability of the vector as a remotely triggered drug delivery system for biomedical applications. Moreover, cell studies in four cell lines showed a subcytotoxic dose of 0.05 mg/mL which was used to analyze the cell metabolism and cell cycle displaying no significant influence in the cell lines studied. In conclusion, CuS@BNC-nanogels presented a promising strategy for the treatment of chronic pain tuning the duration and intensity of the anesthesia by an on-demand externally activated release of the drug.

CRediT authorship contribution statement

Teresa Alejo: Investigation, Methodology, Visualization, Writing - original draft. **: . Victor Sebastian:** Formal analysis, Investigation, Writing – review & editing. **Gracia Mendoza:** Formal analysis, Investigation, Writing – review & editing. **Manuel Arruebo:** Conceptualization, Writing – review & editing, Supervision, Funding acquisition.

Declaration of Competing Interest

The authors declare that they have no known competing financial interests or personal relationships that could have appeared to influence the work reported in this paper.

Acknowledgments

The authors thank financial support from the ERC Consolidator Grant program (ERC-2013-CoG-614715, NANOHEDONISM). V.S. acknowledges the financial support from Ministerio de Ciencia, Innovación y Universidades, Programa Retos Investigación, Proyecto REF: RTI2018-099019-A-I00. CIBER-BBN is an initiative funded by the VI National R&D&i Plan 2008–2011 financed by the Instituto de Salud Carlos III with the assistance of the European Regional Development Fund. Authors acknowledge the LMA-INA, Cell Separation and Flow Cytometry, Cell Culture Units from IACS/IIS Aragon (Spain) for offering access to their instruments and expertise. G.M. thanks the support from the Miguel Servet Program (MS19/00092; Instituto de Salud Carlos III).

Appendix A. Supplementary data

Supplementary data to this article can be found online at https://doi.org/10.1016/j.jcis.2021.09.064.

References

[1] G. Joshi, K. Gandhi, N. Shah, J. Gadsden, S.L. Corman, Peripheral nerve blocks in the management of postoperative pain: challenges and opportunities, J. Clin. Anesth. 35 (2016) 524–529.
[2] M.A. Kirksey, S.C. Haskins, J. Cheng, S.S. Liu, Local Anesthetic Peripheral Nerve Block Adjuvants for Prolongation of Analgesia: A Systematic Qualitative Review, PLoS ONE 10 (2015) e0137312.
[3] D.E. Becker, K.L. Reed, Local anesthetics: review of pharmacological considerations, Anesth. Prog. 59 (2012) 90–103.

[4] D.R. de Araújo, L.N.d.M. Ribeiro, E. de Paula, Lipid-based carriers for the delivery of local anesthetics, Expert Opin. Drug Deliv. 16 (2019) 701–714.
[5] Y.H. Yun, B.K. Lee, K. Park, Controlled Drug Delivery: Historical perspective for the next generation, J. Control. Release 219 (2015) 2–7.
[6] V. Andreu, M. Arruebo, Current progress and challenges of nanoparticle-based therapeutics in pain management, J. Control. Release 269 (2018) 189–213.
[7] A.Y. Rwei, J.J. Lee, C. Zhan, Q. Liu, M.T. Ok, S.A. Shankarappa, R. Langer, D.S. Kohane, Repeatable and adjustable on-demand sciatic nerve block with phototriggerable liposomes, Proc. Natl. Acad. Sci. USA 112 (2015) 15719–15724.
[8] B.P. Timko, T. Dvir, D.S. Kohane, Remotely Triggerable Drug Delivery Systems, Adv. Mater. 22 (2010) 4925–4943.
[9] Y. Wang, D.S. Kohane, External triggering and triggered targeting strategies for drug delivery, Nat. Rev. Mater. 2 (2017) 17020.
[10] M. Karimi, A. Ghasemi, P. Sahandi Zangabad, R. Rahighi, S.M. Moosavi Basri, H. Mirshekari, M. Amiri, Z. Shafaei Pishabad, A. Aslani, M. Bozorgomid, D. Ghosh, A. Beyzavi, A. Vaseghi, A.R. Aref, L. Haghani, S. Bahrami, M.R. Hamblin, Smart micro/nanoparticles in stimulus-responsive drug/gene delivery systems, Chem. Soc. Rev. 45 (2016) 1457–1501.
[11] W.F. Cheong, S.A. Prahl, A.J. Welch, A review of the optical properties of biological tissues, IEEE J. Quantum Electron. 26 (1990) 2166–2185.
[12] C. Ash, M. Dubec, K. Donne, T. Bashford, Effect of wavelength and beam width on penetration in light-tissue interaction using computational methods, Lasers Med. Sci. 32 (2017) 1909–1918.
[13] B.E. Smith, P.B. Roder, X. Zhou, P.J. Pauzauskie, Nanoscale materials for hyperthermal theranostics, Nanoscale 7 (2015) 7115–7126.
[14] J. Chen, C. Ning, Z. Zhou, P. Yu, Y. Zhu, G. Tan, C. Mao, Nanomaterials as photothermal therapeutic agents, Prog. Mater. Sci. 99 (2019) 1–26.
[15] I. Ortiz de Solorzano, T. Alejo, M. Abad, C. Bueno-Alejo, G. Mendoza, V. Andreu, S. Irusta, V. Sebastian, M. Arruebo, Cleavable and thermo-responsive hybrid nanoparticles for on-demand drug delivery, J. Colloid Interface Sci. 533 (2019) 171–181.
[16] T. Alejo, M. Prieto, H. García-Juan, V. Andreu, G. Mendoza, V. Sebastián, M. Arruebo, A facile method for the controlled polymerization of biocompatible and thermoresponsive oligo(ethylene glycol) methyl ether methacrylate copolymers, Polym. J. 50 (2018) 203–211.
[17] J.-F. Lutz, A. Hoth, Preparation of Ideal PEG Analogues with a Tunable Thermosensitivity by Controlled Radical Copolymerization of 2-(2-Methoxyethoxy)ethyl Methacrylate and Oligo(ethylene glycol) Methacrylate, Macromolecules 39 (2006) 893–896.
[18] C. Wang, X. Liu, V. Wulf, M. Vazquez-Gonzalez, M. Fadeev, I. Willner, DNA-Based Hydrogels Loaded with Au Nanoparticles or Au Nanorods: Thermoresponsive Plasmonic Matrices for Shape-Memory, Self-Healing, Controlled Release, and Mechanical Applications, ACS Nano 13 (2019) 3424–3433.
[19] J. You, P. Zhang, F. Hu, Y. Du, H. Yuan, J. Zhu, Z. Wang, J. Zhou, C. Li, Near-Infrared Light-Sensitive Liposomes for the Enhanced Photothermal Tumor Treatment by the Combination with Chemotherapy, Pharm. Res. 31 (2014) 554–565.
[20] D.S. Chauhan, R. Prasad, J. Devrukhkar, K. Selvaraj, R. Srivastava, Disintegrable NIR Light Triggered Gold Nanorods Supported Liposomal Nanohybrids for Cancer Theranostics, Bioconjugate Chem. 29 (2018) 1510–1518.
[21] Y. Xia, W. Li, C.M. Cobley, J. Chen, X. Xia, Q. Zhang, M. Yang, E.C. Cho, P.K. Brown, Gold Nanocages: From Synthesis to Theranostic Applications, Acc. Chem. Res 44 (2011) 914–924.
[22] M.S. Yavuz, Y. Cheng, J. Chen, C.M. Cobley, Q. Zhang, M. Rycenga, J. Xie, C. Kim, K.H. Song, A.G. Schwartz, L.V. Wang, Y. Xia, Gold nanocages covered by smart polymers for controlled release with near-infrared light, Nat. Mater. 8 (2009) 935–939.
[23] I. Ortiz de Solorzano, G. Mendoza, M. Arruebo, V. Sebastian, Customized hybrid and NIR-light triggered thermoresponsive drug delivery microparticles synthetized by photopolymerization in a one-step flow focusing continuous microreactor, Colloids Surf. B. 190 (2020) 110904.
[24] I.O. de Solorzano, M. Prieto, G. Mendoza, V. Sebastian, M. Arruebo, Triggered drug release from hybrid thermoresponsive nanoparticles using near infrared light, Nanomedicine 15 (2019) 219–234.
[25] T. Alejo, V. Andreu, G. Mendoza, V. Sebastian, M. Arruebo, Controlled release of bupivacaine using hybrid thermoresponsive nanoparticles activated via photothermal heating, J. Colloid Interface Sci. 523 (2018) 234–244.
[26] T. Yildiz, R.P. Gu, S. Zauscher, T. Betancourt, Doxorubicin-loaded protease-activated near-infrared fluorescent polymeric nanoparticles for imaging and therapy of cancer, Int. J. Nanomed. 13 (2018) 6961–6986.
[27] L. Ruiz-Gaton, S. Espuelas, J. Huarte, E. Larraneta, N. Martin-Arbella, J.M. Irache, Nanoparticles from Gantrez (R) AN-poly(ethylene glycol) conjugates as carriers for oral delivery of docetaxel, Int. J. Pharm. 571 (2019) 10.
[28] K. Joshi, A. Chandra, K. Jain, S. Talegaonkar, Nanocrystalization: An Emerging Technology to Enhance the Bioavailability of Poorly Soluble Drugs, Pharm. Nanotechnol. 7 (2019) 259–278.
[29] T. Alejo, L. Uson, G. Landa, M. Prieto, C. Yus Argon, S. Garcia-Salinas, R. de Miguel, A. Rodriguez-Largo, S. Irusta, V. Sebastian, G. Mendoza, M. Arruebo, Nanogels with High Loading of Anesthetic Nanocrystals for Extended Duration of Sciatic Nerve Block, ACS Appl, Mater. Interfaces 13 (2021) 17220–17235.
[30] H. Parshad, K. Frydenvang, T. Liljefors, C. Cornett, C. Larsen, Assessment of drug salt release from solutions, suspensions and in situ suspensions using a rotating dialysis cell, Eur. J. Pharm. Sci. 19 (2003) 263–272.
[31] S. Ramadan, L. Guo, Y. Li, B. Yan, W. Lu, Hollow Copper Sulfide Nanoparticle-Mediated Transdermal Drug Delivery, Small 8 (2012) 3143–3150.
[32] M. Karg, I. Pastoriza-Santos, J. Pérez-Juste, T. Hellweg, L.M. Liz-Marzán, Nanorod-Coated PNIPAM Microgels: Thermoresponsive Optical Properties, Small 3 (2007) 1222–1229.
[33] A.B. Moustafa, R.A. Sobh, A.M. Rabie, H.E. Nasr, M.M.H. Ayoub, Differential microemulsion polymerization as a new root for entrapment of drugs, J. Appl. Polym. Sci. 127 (2013) 4634–4643.
[34] L. Gomez, V. Sebastian, S. Irusta, A. Ibarra, M. Arruebo, J. Santamaria, Scaled-up production of plasmonic nanoparticles using microfluidics: from metal precursors to functionalized and sterilized nanoparticles, Lab Chip 14 (2014) 325–332.
[35] I. Ortiz de Solorzano, M. Prieto, G. Mendoza, T. Alejo, S. Irusta, V. Sebastian, M. Arruebo, Microfluidic Synthesis and Biological Evaluation of Photothermal Biodegradable Copper Sulfide Nanoparticles, ACS Appl. Mater. Interfaces 8 (2016) 21545–21554.
[36] M.L. Martins, J. Eckert, H. Jacobsen, E.C. dos Santos, R. Ignazzi, D.R. de Araujo, M.-C. Bellissent-Funel, F. Natali, M. Marek Koza, A. Matic, E. de Paula, H.N. Bordallo, Raman and Infrared spectroscopies and X-ray diffraction data on bupivacaine and ropivacaine complexed with 2-hydroxypropyl−β−cyclodextrin, Data Brief 15 (2017) 25–29.
[37] Y. Wang, Y. Shen, Y. Zhang, B. Yue, C. Wu, pH-Sensitive Polyacrylic Acid (PAA) Hydrogels Trapped with Polysodium-p-Styrenesulfonate (PSS), J. Macromol. Sci. B 45 (2006) 563–571.
[38] S. Riyaz, A. Parveen, A. Azam, Microstructural and optical properties of CuS nanoparticles prepared by sol–gel route, Perspect. Sci 8 (2016) 632–635.
[39] H.S. Kim, D.Y. Lee, Near-Infrared-Responsive Cancer Photothermal and Photodynamic Therapy Using Gold Nanoparticles, Polymers 10 (2018) 961.
[40] X.W. Qu, P.H. Qiu, Y. Zhu, M.Y. Yang, C.B. Mao, Guiding nanomaterials to tumors for breast cancer precision medicine: from tumor-targeting small-molecule discovery to targeted nanodrug delivery, NPG Asia Mater. 9 (2017) e452.
[41] Q.F. Ban, T. Bai, X. Duan, J. Kong, Noninvasive photothermal cancer therapy nanoplatforms via integrating nanomaterials and functional polymers, Biomater. Sci. 5 (2017) 190–210.
[42] E. Cazares-Cortes, A. Espinosa, J.M. Guigner, A. Michel, N. Griffete, C. Wilhelm, C. Menager, Doxorubicin Intracellular Remote Release from Biocompatible Oligo(ethylene glycol) Methyl Ether Methacrylate-Based Magnetic Nanogels Triggered by Magnetic Hyperthermia, ACS Appl. Mater. Interfaces 9 (2017) 25775–25788.
[43] T. Alejo, L. Uson, M. Arruebo, Reversible stimuli-responsive nanomaterials with on-off switching ability for biomedical applications, J. Control. Release 314 (2019) 162–176.
[44] C. Zhan, W. Wang, J.B. McAlvin, S. Guo, B.P. Timko, C. Santamaria, D.S. Kohane, Phototriggered Local Anesthesia, Nano Lett. 16 (2016) 177–181.
[45] S. Bancos, D.L. Stevens, K.M. Tyner, Effect of silica and gold nanoparticles on macrophage proliferation, activation markers, cytokine production, and phagocytosis in vitro, Int. J. Nanomed. 10 (2015) 183–206.
[46] C.F. Jones, D.W. Grainger, In vitro assessments of nanomaterial toxicity, Adv. Drug Deliv. Rev. 61 (2009) 438–456.
[47] ISO 10993-5:2009 - Biological Evaluation of Medical Devices. Part 5: Tests for In Vitro Cytotoxicity. http://www.iso.org/iso/catalogue_detail.htm?csnumber=36406. [Accessed: 17- March- 2021].